Bayesian Multi-Snapshot Learning for Sparse Doubly-Selective CSI Estimation in DCO-OTFS VLC Systems

Shubham Saxena[⋆], Suraj Srivastava[‡], and Aditya K. Jagannatham[⋆]
[⋆]Department of Electrical Engineering, Indian Institute of Technology Kanpur, India
[‡]Department of Electrical Engineering, Indian Institute of Technology Jodhpur, India
Email: [⋆]{shubs20, adityaj}@iitk.ac.in, [‡]{surajsri}@iitj.ac.in

***Abstract*—A novel channel impulse response (CIR) estimation framework is proposed for direct-current-biased optical orthogonal time-frequency space (DCO-OTFS) modulated visible light communication (VLC) systems operating over doubly-selective channels. The approach leverages simultaneous sparsity across multiple snapshots to estimate the delay-Doppler (DD)-domain CIR by transmitting pilot symbols directly over the time-frequency (TF) grid. This design minimizes pilot overhead and training duration while eliminating the need for DD-domain guard intervals between pilot and data symbols, thereby enhancing spectral efficiency. Conventional and compressive sensing-based channel estimation (CE) schemes are complemented by the proposed DD Bayesian Multiple-snapshot Learning (DD-BML) for DCO-OTFS estimator, which leverages joint DD-domain sparsity to enhance estimation accuracy. A low-complexity linear minimum mean square error (LMMSE) detector is then employed for data detection. Additionally, benchmark estimators such as the Oracle-based minimum mean square error (OMMSE) and Bayesian Cramer-Rao lower bound (BCRLB) are derived for performance comparison. Simulation results demonstrate that the proposed method yields superior performance in terms of normalized mean-square-error (NMSE), pilot overhead, and bit error-rate (BER).**

I. Introduction

Escalating traffic and limited radio-frequency (RF) spectrum have driven intense interest in visible light communication (VLC) as a complementary access technology [1], [2]. VLC employs light-emitting diodes (LEDs) and photodiodes (PDs) for high-rate indoor links [1], [2]. Practical VLC channels include line-of-sight (LoS) and reflected non-LoS (NLoS) components whose delay dispersion causes inter-symbol interference (ISI) [1], [2]. Accordingly, optical orthogonal frequency division multiplexing (O-OFDM) remains a prevalent baseline to suppress ISI with low-complexity equalization [1], [2]. Orthogonal time frequency space (OTFS) has been advanced for delay-Doppler (DD) selective channels, where DD-domain processing enables robust detection and structured channel estimation (CE) [3], [4]. These properties motivated optical OTFS (O-OTFS) for VLC [5]. To satisfy intensity modulation/direct detection (IM/DD) constraints, Zhong *et al.* proposed direct-current-biased O-OTFS (DCO-OTFS) using two-dimensional (2D) Hermitian symmetry, reporting improved bit error-rate (BER) and peak-to-average power ratio versus O-OFDM [5]. In [6], Zheng *et al.* proposed a full-duplex relay-assisted VLC system based on DCO-OTFS, demonstrating reduced cyclic-prefix (CP) overhead in comparison with DCO-OFDM. Further advancements were presented by Sharma *et al.* [7], who developed a hyperparameter-free receiver employing random Fourier features (RFF) for O-OTFS modulation in VLC systems to mitigate transmitter nonlinearity. Xu *et al.* in [1] introduced O-OTFS, which enhances bandwidth, power, and energy efficiency over O-OFDM while enabling DD-domain CE. Similarly, Cai *et al.* [8] designed a power- and spectrum-efficient O-OTFS framework tailored for underwater VLC systems. Chen *et al.* in [9] proposed an IM/DD-based satellite communication scheme utilizing DCO-OTFS to counteract fading and Doppler effects, achieving superior bandwidth, power, and hardware efficiency compared to DCO-OFDM. Moreover, Liao *et al.* [10] established the input-output relationship between CSI and received pilot symbols in the DD-domain, proposing a sparse Bayesian learning (BL) CE approach incorporating embedded pilots for O-OTFS VLC. However, most existing studies rely on DD-domain guard intervals for pilot placement, reducing spectral efficiency. Motivated by these limitations, this work introduces a novel DD Bayesian multiple-snapshot learning (DD-BML) CE framework for DCO-OTFS VLC systems. The proposed method directly transmits pilot symbols in the time-frequency (TF) domain, thereby minimizing pilot overhead and training time while eliminating DD-domain guard intervals to enhance overall spectral efficiency.

In this context, this study develops an simultaneously sparse CE scheme based on the multiple snapshots for the DCO-OTFS VLC system, wherein pilot symbols are directly transmitted within the TF-domain. This design effectively minimizes pilot overhead, training duration, and pre-processing complexity. The proposed CE model further eliminates the need for a DD-domain guard interval between pilot and data symbols, thereby enhancing overall bandwidth efficiency. Furthermore, a novel DD-BML framework is introduced, which effectively exploits DD-domain sparsity to achieve enhanced CSI estimation. The proposed approach eliminates the need for hyperparameter optimization, thereby ensuring consistent structural precision and robust convergence. The efficiency of our DD-BML-based method is further characterized by deriving closed-form expressions for both the Oracle-based minimum mean square error (OMMSE) estimator and for the Bayesian Cramer-Rao lower bound (BCRLB). Finally, the proposed DD-BML approach is validated in terms of BER, NMSE, and pilot overhead, demonstrating clear improvements over existing techniques in DCO-OTFS VLC systems.

Notations: Bold lowercase and uppercase denote column vectors and matrices, with indices starting at 0. The operator $\mathrm{vec}(\mathbf{A})$ stacks the columns of $\mathbf{A}$ into a vector, and $\mathrm{vec}^{-1}(\mathbf{a})$ performs the inverse mapping. We use $\mathrm{vec}(\mathbf{ABC}) = (\mathbf{C}^T \otimes \mathbf{A})\mathrm{vec}(\mathbf{B})$, where $\otimes$ denotes the Kronecker product.

II. DCO-OTFS VLC System Model

Consider a DCO-OTFS system characterized by frame duration $T_d = NT$ and bandwidth $B = M\Delta f$, where T and Δf

denote the symbol period and subcarrier spacing, respectively, satisfying $T\Delta f = 1$. The parameters N and M specify the number of symbols along the time and frequency dimensions of the TF-grid. In DCO-OTFS, data symbols are mapped onto an equivalent DD-grid, where the Doppler and delay domains are discretized with sampling intervals $\Delta\nu = \frac{1}{T_d}$ and $\Delta\tau = \frac{1}{B}$.

A. DCO-OTFS Modulation

Let $\mathbf{S}_{\rm dd} \in \mathbb{C}^{M\times N}$ represent the matrix of transmitted information symbols, where each element $\mathbf{S}_{\rm dd}(l,\tilde{k})$ corresponds to the symbol mapped onto the delay index l, $0 \le l \le M-1$ and Doppler index $\tilde{k}$, $0 \le \tilde{k} \le N-1$. 2D Hermitian symmetry is applied to guarantee that the generated waveform remains real-valued, given as [1], [6], [9]

$$\mathbf{S}_{\rm dd}(l,\tilde{k}) = \begin{cases} \mathbf{S}_{\rm dd}(l,\tilde{k}), & \tilde{k} = 1,2,\ldots,\frac{N}{2}-1, \\ \mathbf{S}^*_{\rm dd}(l,N-\tilde{k}), & \tilde{k} = \frac{N}{2}+1,\ldots,N-1, \\ 0, & \tilde{k} = 0,\frac{N}{2}. \end{cases} \quad (1)$$

Subsequently, the transmitter converts the DD-domain symbols into their TF-domain counterparts through the inverse symplectic finite Fourier transform (ISFFT), defined as [1]

$$\mathbf{S}_{\rm tf}(m,n) = \frac{1}{\sqrt{NM}} \sum_{l=0}^{M-1}\sum_{\tilde{k}=0}^{N-1} \mathbf{S}_{\rm dd}(l,\tilde{k}) e^{j2\pi\left(\frac{n\tilde{k}}{N} - \frac{ml}{M}\right)}, \quad (2)$$

where the matrix $\mathbf{S}_{\rm tf} \in \mathbb{C}^{M\times N}$ represents the TF-domain symbol matrix, with its (m,n)-th entry $\mathbf{S}_{\rm tf}(m,n)$ indicating the symbol transmitted through the m-th subcarrier during the n-th symbol interval. The matrix expression in (2) can thus be equivalently formulated as $\mathbf{S}_{\rm tf} = \mathbf{F}_M \mathbf{S}_{\rm dd} \mathbf{F}_N^H$, where $\mathbf{F}_M$ and $\mathbf{F}_N$ denotes the unitary discrete Fourier transform (DFT) matrix. The time-domain (TD) signal is subsequently derived by applying the Heisenberg transform to the TF-domain symbol matrix $\mathbf{S}_{\rm tf}$. Let $p_s(t)$ represent the transmit pulse of duration T, repeated N times within the DCO-OTFS frame period T_d. Accordingly, the transmit signal matrix $\mathbf{X} \in \mathbb{R}^{M\times N}$ is given as

$$\mathbf{X} = \mathbf{P}_{\rm s}\mathbf{F}_M^H \mathbf{S}_{\rm tf} = \mathbf{P}_{\rm s}\mathbf{S}_{\rm dd}\mathbf{F}_N^H, \quad (3)$$

where $\mathbf{P}_{\rm s} = \mathrm{diag}\{p_s(\frac{pT}{M})\}_{p=0}^{M-1} \in \mathbb{R}^{M\times M}$ [1], [8]. Moreover, the MN-sample transmit signal $\mathbf{x} \in \mathbb{R}^{MN\times 1}$ is

$$\mathbf{x} = \mathrm{vec}\left(\mathbf{P}_{\rm s}\mathbf{S}_{\rm dd}\mathbf{F}_N^H\right) = \left(\mathbf{F}_N^H \otimes \mathbf{P}_{\rm s}\right)\mathbf{s}_{\rm dd}, \quad (4)$$

where $\mathbf{s}_{\rm dd} = \mathrm{vec}(\mathbf{S}_{\rm dd}) \in \mathbb{C}^{MN\times 1}$ [1], [8]. Prior to transmission, a cyclic prefix (CP) of length L is appended to mitigate inter-frame interference. Furthermore, a suitable DC bias is added to ensure the optical intensity is nonnegative; the biasing/clipping operation is omitted here for brevity. The next subsection describes the DD-domain VLC channel model.

B. DD-Domain VLC Channel Model

Let $h(\tau,\nu)$ denote the DD-domain representation of the VLC channel, expressed as a two-dimensional function of the delay variable τ and Doppler variable ν, corresponding to a doubly-selective VLC propagation environment. Owing to the limited number of dominant reflectors in practical VLC environments, the DD-domain channel can be modeled as a sparse superposition of discrete propagation paths, given by

$$h(\tau,\nu) = \sum_{i=1}^{L_p} h_i\,\delta(\tau-\tau_i)\,\delta(\nu-\nu_i), \quad (5)$$

where $h_i \in \mathbb{R}$ represents the VLC channel coefficients corresponding to the ith propagation path, $\tau_i = \frac{l_i}{M\Delta f}$ and $\nu_i = \frac{\tilde{k}_i}{NT}$ represent the corresponding delay and Doppler shifts, with $l_i < M$ and $\tilde{k}_i < N$ being the integer indices corresponding to the respective delay and Doppler positions [3], [4], [7]. The parameter L_p indicates the total number of dominant multipath components, while $\delta(\cdot)$ denotes the Dirac delta function. Since reflected VLC channel coefficients experience higher attenuation with increasing delay, the channel coefficients are modeled as an exponentially decaying function across the DCO-OTFS delay bins [2], [10]. The magnitude of the ith channel tap is then expressed as

$$h_i = \frac{e^{-l_i\Delta\tau/\tau_{\rm rms}}}{\sum_{n=0}^{L_p-1} e^{-n\Delta\tau/\tau_{\rm rms}}}, \quad (6)$$

where $l_i \in \{0,1,\ldots,L_p-1\}$ is the delay-bin index of the ith path and $\tau_{\rm rms}$ denotes the channel's root-mean-square (RMS) delay spread [2], [10]. Typically, $\tau_{\rm rms} \in [0.5\Delta\tau,\, 1.5\Delta\tau]$, and its value depends on the average surface reflectivity and room geometry [2], [10].

C. DCO-OTFS Demodulation

Let $\mathbf{r} \in \mathbb{C}^{MN\times 1}$ and $\mathbf{n} \in \mathbb{C}^{MN\times 1}$ represent the received signal vector and the additive noise vector after CP removal, respectively. The received signal $\mathbf{r}$ is as follows [3], [4]

$$\mathbf{r} = \widetilde{\mathbf{H}}\mathbf{x} + \mathbf{n}, \quad (7)$$

where the channel matrix $\widetilde{\mathbf{H}} \in \mathbb{C}^{MN\times MN}$ is expressed as $\widetilde{\mathbf{H}} = \sum_{i=1}^{L_p} h_i \mathbf{\Psi}^{l_i}\mathbf{\Lambda}^{\tilde{k}_i}$. Here, $\mathbf{\Psi} \in \mathbb{R}^{MN\times MN}$ represents the permutation matrix and $\mathbf{\Lambda} = \mathrm{diag}\{\omega^i\}_{i=0}^{MN-1} \in \mathbb{C}^{MN\times MN}$, with $\omega = e^{j2\pi/MN}$ [3], [4]. Let $\mathbf{Y}_{\rm tf} \in \mathbb{C}^{M\times N}$ denote the TF-domain demodulated symbol matrix. It is obtained from the discrete Wigner transform of the received sample matrix $\mathbf{R} = \mathrm{vec}^{-1}(\mathbf{r}) \in \mathbb{C}^{M\times N}$, expressed as $\mathbf{Y}_{\rm tf} = \mathbf{F}_M\mathbf{P}_{\rm r}\mathbf{R}$, where $\mathbf{P}_{\rm r} = \mathrm{diag}\{p^*_{\rm r}(\frac{pT}{M})\}_{p=0}^{M-1}$ and $p_{\rm r}(t)$ denotes the receiver pulse of duration T [3], [4], [6]. The DD-domain matrix $\mathbf{Y}_{\rm dd} \in \mathbb{C}^{M\times N}$ is obtained by applying the symplectic finite Fourier transform (SFFT) to $\mathbf{Y}_{\rm tf}$, expressed as [3], [4]

$$\mathbf{Y}_{\rm dd} = \mathbf{F}_M^H\mathbf{Y}_{\rm tf}\mathbf{F}_N = \mathbf{P}_{\rm r}\mathbf{R}\mathbf{F}_N. \quad (8)$$

The vectorized form of (8) is $\mathbf{y}_{\rm dd} = \mathrm{vec}(\mathbf{Y}_{\rm dd}) \in \mathbb{C}^{MN\times 1}$

$$\mathbf{y}_{\rm dd} = \left(\mathbf{F}_N \otimes \mathbf{P}_{\rm r}\right)\mathbf{r}. \quad (9)$$

Substituting $\mathbf{r}$ from (7) and $\mathbf{x}$ from (4) into (9) yields the DD-domain DCO-OTFS model as [3], [4]

$$\mathbf{y}_{\rm dd} = \mathbf{H}_{\rm dd}\mathbf{s}_{\rm dd} + \mathbf{v}_{\rm dd}, \quad (10)$$

where $\mathbf{H}_{\rm dd} = (\mathbf{F}_N \otimes \mathbf{P}_{\rm r})\widetilde{\mathbf{H}}(\mathbf{F}_N^H \otimes \mathbf{P}_{\rm s}) \in \mathbb{C}^{MN\times MN}$ and $\mathbf{v}_{\rm dd} = (\mathbf{F}_N \otimes \mathbf{P}_{\rm r})\mathbf{n} \in \mathbb{C}^{MN\times 1}$. Assuming unit average symbol power, the linear minimum mean square error (LMMSE)-based detection is expressed as [2]

$$\widehat{\mathbf{s}}_{\rm dd}^{\rm LMMSE} = \left(\mathbf{H}_{\rm dd}^H\mathbf{R}_{v,\rm dd}^{-1}\mathbf{H}_{\rm dd} + \mathbf{I}_{MN}\right)^{-1}\mathbf{H}_{\rm dd}^H\mathbf{R}_{v,\rm dd}^{-1}\mathbf{y}_{\rm dd}, \quad (11)$$

where $\mathbf{R}_{v,\rm dd} = \sigma^2[\mathbf{I}_N \otimes (\mathbf{P}_{\rm r}\mathbf{P}_{\rm r}^H)] \in \mathbb{C}^{MN\times MN}$ represents the covariance matrix of the noise vector $\mathbf{v}_{\rm dd}$ with σ^2 as the noise

variance. As previously discussed, precise CSI estimation is essential for harnessing the full potential of the DCO-OTFS VLC system, which constitutes the focus of the next section.

III. Simultaneous Sparse DD-domain CE

Let $\mathbf{S}_{\mathrm{tf},\mathcal{P}} \in \mathbb{C}^{M\times N_p}$ represent the TF-domain pilot matrix, where N_p denotes the total number of pilot symbols distributed along the time axis. Consequently, based on (3), the TD pilot sample matrix is $\mathbf{X}_{\mathcal{P}} = \mathbf{P}_{\mathrm{s}}\mathbf{F}_M^H\mathbf{S}_{\mathrm{tf},\mathcal{P}} \in \mathbb{R}^{M\times N_p}$. Let $h_j^i \in \mathbb{R}_+$ denote the gain corresponding to the ith delay tap and jth Doppler tap, where $0 \le i \le M_\tau - 1$ and $0 \le j \le N_\nu - 1$. The parameters M_τ and N_ν define the grid resolutions along the delay and Doppler dimensions, respectively, used for the sparse characterization of the DD-domain CSI, satisfying $\max(l_i) < M_\tau \ll M$ and $\max(\tilde{k}_i) < N_\nu \ll N$. Thus, the sparse DD-domain channel $h(\tau,\nu)$ in (5) is given by [4], [7]

$$h(\tau,\nu) = \sum_{i=0}^{M_\tau-1}\sum_{j=0}^{N_\nu-1} h_j^i\delta(\tau-\tau_i)\delta(\nu-\nu_j), \tag{12}$$

where $\tau_i = \frac{i}{M\Delta f}$ and $\nu_j = \frac{j}{NT}$. Owing to the presence of only a limited number of dominant reflectors in the wireless channel, merely a few coefficients L_p remain non-zero among the total $M_\tau N_\nu$ components. After eliminating the CP, the received TD pilot vector $\mathbf{r}_{\mathcal{P}} \in \mathbb{C}^{MN_p\times 1}$ can be expressed as

$$\mathbf{r}_{\mathcal{P}} = \bar{\mathbf{H}}\mathbf{x}_{\mathcal{P}} + \mathbf{n}_{\mathcal{P}}, \tag{13}$$

where $\mathbf{x}_{\mathcal{P}} = \mathrm{vec}(\mathbf{X}_{\mathcal{P}}) \in \mathbb{R}^{MN_p\times 1}$, and $\mathbf{n}_{\mathcal{P}} \in \mathbb{C}^{MN_p\times 1}$ denotes the noise vector. The matrix $\bar{\mathbf{H}} \in \mathbb{C}^{MN_p\times MN_p}$ is

$$\bar{\mathbf{H}} = \sum_{i=0}^{M_\tau-1}\sum_{j=0}^{N_\nu-1} h_j^i\left(\bar{\mathbf{\Psi}}\right)^i\left(\bar{\mathbf{\Lambda}}_i\right)^j, \tag{14}$$

where $\bar{\mathbf{\Psi}}$ represents a permutation matrix of dimension $MN_p \times MN_p$, and $\bar{\mathbf{\Lambda}}_i \in \mathbb{C}^{MN_p\times MN_p}$ is given as [3], [4]

$$\bar{\mathbf{\Lambda}}_i = \begin{cases} \mathrm{diag}\left\{1,\omega,\ldots,\omega^{MN_p-i-1},\omega^{-i},\ldots,\omega^{-1}\right\}, \text{if } i\neq 0,\\ \mathrm{diag}\left\{1,\omega,\ldots,\omega^{MN_p-1}\right\}, \text{for } i=0. \end{cases} \tag{15}$$

Let the received pilot matrix $\mathbf{R}_{\mathcal{P}} \in \mathbb{C}^{M\times N_p}$ be defined as $\mathbf{R}_{\mathcal{P}} = \mathrm{vec}^{-1}(\mathbf{r}_{\mathcal{P}})$. Accordingly, the TF-domain pilot symbol matrix $\mathbf{Y}_{\mathrm{tf},\mathcal{P}} \in \mathbb{C}^{M\times N_p}$ can be expressed as $\mathbf{Y}_{\mathrm{tf},\mathcal{P}} = \mathbf{F}_M\mathbf{P}_{\mathrm{r}}\mathbf{R}_{\mathcal{P}}$. The corresponding vectorized form is given as

$$\mathbf{y}_{\mathrm{tf},\mathcal{P}} = \mathrm{vec}(\mathbf{Y}_{\mathrm{tf},\mathcal{P}}) = \left[\mathbf{I}_{N_p}\otimes(\mathbf{F}_M\mathbf{P}_{\mathrm{r}})\right]\mathbf{r}_{\mathcal{P}}. \tag{16}$$

By substituting $\mathbf{r}_{\mathcal{P}}$ from (13) into (16), and replacing $\mathbf{x}_{\mathcal{P}}$, the expression for $\mathbf{y}_{\mathrm{tf},\mathcal{P}}$ can be given as

$$\mathbf{y}_{\mathrm{tf},\mathcal{P}} = \left[\mathbf{I}_{N_p}\otimes(\mathbf{F}_M\mathbf{P}_{\mathrm{r}})\right]\bar{\mathbf{H}}\left[\mathbf{I}_{N_p}\otimes\left(\mathbf{P}_{\mathrm{s}}\mathbf{F}_M^H\right)\right]\mathbf{s}_{\mathrm{tf},\mathcal{P}} + \mathbf{v}, \tag{17}$$

where $\mathbf{s}_{\mathrm{tf},\mathcal{P}} = \mathrm{vec}(\mathbf{S}_{\mathrm{tf},\mathcal{P}}) \in \mathbb{C}^{MN_p\times 1}$ and $\mathbf{v} = [\mathbf{I}_{N_p}\otimes(\mathbf{F}_M\mathbf{P}_{\mathrm{r}})]\mathbf{n}_{\mathcal{P}} \in \mathbb{C}^{MN_p\times 1}$. By substituting $\bar{\mathbf{H}}$ from (14) into the above expression, we obtain [3], [4]

$$\mathbf{y}_{\mathrm{tf},\mathcal{P}} = \sum_{i=0}^{M_\tau-1}\sum_{j=0}^{N_\nu-1}\boldsymbol{\omega}_j^i h_j^i + \mathbf{v}, \tag{18}$$

where $\boldsymbol{\omega}_j^i = [\mathbf{I}_{N_p}\otimes(\mathbf{F}_M\mathbf{P}_{\mathrm{r}})]\,\bar{\mathbf{\Psi}}^i\bar{\mathbf{\Lambda}}_i^j[\mathbf{I}_{N_p}\otimes(\mathbf{P}_{\mathrm{s}}\mathbf{F}_M^{\mathrm{H}})]\mathbf{s}_{\mathrm{tf},\mathcal{P}}$. Consequently, (18) can be reformulated as [3], [4]

$$\mathbf{y}_{\mathrm{tf},\mathcal{P}} = \mathbf{\Phi}\mathbf{h} + \mathbf{v}, \tag{19}$$

where the dictionary matrix $\mathbf{\Phi} \in \mathbb{C}^{MN_p\times M_\tau N_\nu}$ and the vector $\mathbf{h} \in \mathbb{R}_+^{M_\tau N_\nu\times 1}$ are defined as $\mathbf{\Phi} = \left[\boldsymbol{\omega}_0^0,\ \boldsymbol{\omega}_1^0,\ldots,\boldsymbol{\omega}_{N_\nu-1}^0,\ldots,\boldsymbol{\omega}_0^{M_\tau-1},\ldots,\boldsymbol{\omega}_{N_\nu-1}^{M_\tau-1}\right]$ and $\mathbf{h} = \left[h_0^0,h_1^0,\ldots,h_{N_\nu-1}^0,\ldots,h_0^{M_\tau-1},\ldots,h_{N_\nu-1}^{M_\tau-1}\right]^T$.

Consider a case involving multiple pilot output snapshots $\mathbf{y}_{\mathrm{tf},\mathcal{P},k}$, $1 \le k \le K$, generated using an identical transmit pilot matrix $\mathbf{S}_{\mathrm{tf},\mathcal{P}}$. Accordingly, each pilot output can be formulated as $\mathbf{y}_{\mathrm{tf},\mathcal{P},k} = \mathbf{\Phi}\mathbf{h}_k + \mathbf{v}_k$, where k represents the snapshot index. By defining the concatenated matrices $\mathbf{Y}_{\mathrm{tf},\mathcal{P}} = [\mathbf{y}_{\mathrm{tf},\mathcal{P},1}\ \cdots\ \mathbf{y}_{\mathrm{tf},\mathcal{P},K}] \in \mathbb{C}^{MN_p\times K}$, $\mathbf{H} = [\mathbf{h}_1,\ldots,\mathbf{h}_K] \in \mathbb{R}_+^{M_\tau N_\nu\times K}$, and $\mathbf{V} = [\mathbf{v}_1,\ldots,\mathbf{v}_K] \in \mathbb{C}^{MN_p\times K}$, the DD-domain multi-snapshot CSI estimation model is given by

$$\mathbf{Y}_{\mathrm{tf},\mathcal{P}} = \mathbf{\Phi}\mathbf{H} + \mathbf{V}. \tag{20}$$

Considering these K snapshots of the DD-domain CSI $\mathbf{h}_k$ within a geometric coherence time [4], the support set, defined by the L_p indices corresponding to the non-zero elements of $\mathbf{h}_k$, remains invariant [11]. Consequently, the resulting CSI matrix $\mathbf{H}$ exhibits simultaneous sparsity, as all column vectors $\mathbf{h}_k$ share the same sparsity pattern.

Based on the model presented, the conventional sparsity-agnostic (SA) LMMSE estimation for the DCO-OTFS VLC channel can be formulated as follows [2]

$$\widehat{\mathbf{H}}_{\mathrm{LMMSE}} = \left(\mathbf{\Phi}^H\mathbf{R}_v^{-1}\mathbf{\Phi} + \mathbf{R}_h^{-1}\right)^{-1}\mathbf{\Phi}^H\mathbf{R}_v^{-1}\mathbf{Y}_{\mathrm{tf},\mathcal{P}}, \tag{21}$$

where $\mathbf{R}_h \in \mathbb{R}^{M_\tau N_\nu\times M_\tau N_\nu}$ and $\mathbf{R}_v \in \mathbb{C}^{MN_p\times MN_p}$ represent the covariance matrices of the channel vector $\mathbf{h}_k$ and the noise vector $\mathbf{v}_k$, respectively. The noise covariance is expressed as $\mathbf{R}_v = \sigma^2[\mathbf{I}_{N_p}\otimes(\mathbf{F}_M\mathbf{P}_{\mathrm{r}}\mathbf{P}_{\mathrm{r}}^H\mathbf{F}_M^{\mathrm{H}})]$, while the true channel covariance $\mathbf{R}_h$ is generally unknown and is approximated as $\mathbf{I}_{M_\tau N_\nu}$ in (21). It is noteworthy that, despite the widespread use of the conventional SA-LMMSE CE method, it does not leverage the inherent sparsity of the CSI vector $\mathbf{h}$, which contains only a few significant multipath components, a distinctive property of the VLC channel in the DD-domain. To exploit the sparsity, this work proposes a novel DD-BML CE scheme for DCO-OTFS VLC systems.

IV. DD-domain Bayesian multi-snapshot learning (DD-BML)-based DCO-OTFS VLC CIR estimation

In the proposed DD-BML-based framework, the process begins by assigning a parameterized Gaussian prior to the unknown channel vector $\mathbf{h}_k \in \mathbb{R}^{M_\tau N_\nu\times 1}$ [11]. Since the sparsity structure of $\mathbf{h}_k$ remains consistent for $1 \le k \le K$, the joint prior of the simultaneous sparse DD-domain VLC CIR matrix $\mathbf{H}$ can be expressed as [2], [11]

$$f(\mathbf{H};\mathbf{\Gamma}) = \prod_{k=1}^{K}\prod_{i=1}^{M_\tau N_\nu}\frac{1}{\sqrt{2\pi\gamma_i}}\exp\left(-\frac{|h_k(i)|^2}{2\gamma_i}\right), \tag{22}$$

where $\mathbf{\Gamma} = \mathrm{diag}\{\gamma_i\}_{i=1}^{M_\tau N_\nu} \in \mathbb{R}^{M_\tau N_\nu\times M_\tau N_\nu}$ defines the hyperparameter matrix. The corresponding mean and covariance of $\mathbf{h}_k$ are given by [2], [11]

$$\boldsymbol{\mu}_k = \mathbf{\Sigma}\mathbf{\Phi}^H\mathbf{R}_v^{-1}\mathbf{y}_{\mathrm{tf},\mathcal{P},k},\ \mathbf{\Sigma} = \left(\mathbf{\Phi}^H\mathbf{R}_v^{-1}\mathbf{\Phi} + (\widehat{\mathbf{\Gamma}})^{-1}\right)^{-1}. \tag{23}$$

To obtain the mean estimate $\boldsymbol{\mu}_k$, the hyperparameter matrix $\mathbf{\Gamma}$ must first be determined. Consequently, the *a posteriori* distribution of the composite channel matrix $\mathbf{H}$ can be

expressed as $f(\mathbf{H}|\mathbf{Y}_{\mathrm{tf},\mathcal{P}};\mathbf{\Gamma}) \sim \mathcal{CN}(\boldsymbol{\mathcal{M}},\mathbf{\Sigma})$, where $\boldsymbol{\mathcal{M}} = [\boldsymbol{\mu}_1,\boldsymbol{\mu}_2,\ldots,\boldsymbol{\mu}_K] \in \mathbb{C}^{M_\tau N_\nu \times K}$ [2], [11]. If $\gamma_i \to 0$, the ith row of $\mathbf{H}$ tends to zero, as indicated in (22), implying that estimating $\mathbf{H}$ is effectively equivalent to estimating its hyperparameter matrix $\mathbf{\Gamma}$. To achieve this, the log-Bayesian evidence $\log[f(\mathbf{Y}_{\mathrm{tf},\mathcal{P}};\mathbf{\Gamma})]$ is maximized to obtain $\widehat{\mathbf{\Gamma}}$, where $\log[f(\mathbf{Y}_{\mathrm{tf},\mathcal{P}};\mathbf{\Gamma})] = -MN_PK\log(\pi) - K\log(\det(\mathbf{R}_v)) - \sum_{k=1}^{K}(\mathbf{y}_{\mathrm{tf},\mathcal{P},k}-\mathbf{\Phi}\mathbf{h}_k)^H\mathbf{R}_v^{-1}(\mathbf{y}_{\mathrm{tf},\mathcal{P},k}-\mathbf{\Phi}\mathbf{h}_k)$. However, direct maximization of $\log[f(\mathbf{Y}_{\mathrm{tf},\mathcal{P}};\mathbf{\Gamma})]$ is difficult due to its non-convex form, which contains multiple local optima [11].

To tackle this computational challenge, the expectation-maximization (EM) framework is utilized to iteratively optimize $\log[f(\mathbf{Y}_{\mathrm{tf},\mathcal{P}};\mathbf{\Gamma})]$. Due to its inherent properties, each EM iteration guarantees a non-decreasing objective sequence, ensuring convergence of the log-likelihood to a stable value [11]. The convergence robustness of the EM algorithm, combined with the structured prior $f(\mathbf{H};\mathbf{\Gamma})$ embedded in the proposed DD-BML formulation, enhances the accuracy of DD CIR estimation in the DCO-OTFS VLC system. The subsequent steps of the estimation process are as follows. The complete data set is represented by $\{\mathbf{Y}_{\mathrm{tf},\mathcal{P}},\mathbf{H}\}$, and the hyperparameter estimate from the $(j-1)$th EM iteration is expressed as $\widehat{\mathbf{\Gamma}}^{(j-1)} = \mathrm{diag}\{\widehat{\gamma}_i^{(j-1)}\}_{i=1}^{M_\tau N_\nu}$. The procedure for updating the hyperparameter estimate $\widehat{\mathbf{\Gamma}}^{(j)}$ during the jth iteration is formalized in Theorem 1.

Theorem 1: During the jth EM iteration, the hyperparameter update $\widehat{\gamma}_i^{(j)}$, which maximizes the conditional expectation of the log-likelihood for a given $\widehat{\gamma}_i^{(j-1)}$, where $1 \le i \le M_\tau N_\nu$, corresponding to the complete data set, is given as

$$\mathcal{L}\left(\mathbf{\Gamma}|\widehat{\mathbf{\Gamma}}^{(j-1)}\right) = \mathbb{E}_{\mathbf{H}|\mathbf{Y}_{\mathrm{tf},\mathcal{P}};\widehat{\mathbf{\Gamma}}^{(j-1)}}\left\{\log\left[f\left(\mathbf{Y}_{\mathrm{tf},\mathcal{P}},\mathbf{H};\mathbf{\Gamma}\right)\right]\right\},$$

$$\text{yielding, } \widehat{\gamma}_i^{(j)} = \mathbf{\Sigma}^{(j)}(i,i) + \frac{1}{K}\sum_{k=1}^{K}\left|\boldsymbol{\mathcal{M}}^{(j)}(i,k)\right|^2. \tag{24}$$

Proof: The expectation-step (E-step) computes the expected log-likelihood as

$$\begin{aligned}\mathcal{L}\left(\mathbf{\Gamma}|\widehat{\mathbf{\Gamma}}^{(j-1)}\right) &= \mathbb{E}_{\mathbf{H}|\mathbf{Y}_{\mathrm{tf},\mathcal{P}};\widehat{\mathbf{\Gamma}}^{(j-1)}}\left\{\log f(\mathbf{Y}_{\mathrm{tf},\mathcal{P}},\mathbf{H};\mathbf{\Gamma})\right\}\\ &= \mathbb{E}_{\mathbf{H}|\mathbf{Y}_{\mathrm{tf},\mathcal{P}};\widehat{\mathbf{\Gamma}}^{(j-1)}}\left\{\log f(\mathbf{Y}_{\mathrm{tf},\mathcal{P}}|\mathbf{H}) + \log f(\mathbf{H};\mathbf{\Gamma})\right\} \end{aligned}\tag{25}$$

Since $\mathbb{E}_{\mathbf{H}|\mathbf{Y}_{\mathrm{tf},\mathcal{P}};\widehat{\mathbf{\Gamma}}^{(j-1)}}\{\log f(\mathbf{Y}_{\mathrm{tf},\mathcal{P}}|\mathbf{H})\}$ is independent of $\mathbf{\Gamma}$, the maximization step (M-step) maximizes only the term involving $f(\mathbf{H};\mathbf{\Gamma})$, yielding

$$\begin{aligned}\widehat{\mathbf{\Gamma}}^{(j)} &= \arg\max_{\mathbf{\Gamma}}\mathbb{E}_{\mathbf{H}|\mathbf{Y}_{\mathrm{tf},\mathcal{P}};\widehat{\mathbf{\Gamma}}^{(j-1)}}\{\log f(\mathbf{H};\mathbf{\Gamma})\}\\ &= \arg\max_{\mathbf{\Gamma}}\sum_{i=1}^{M_\tau N_\nu}\left(-K\log(\gamma_i) - \frac{1}{\gamma_i}\sum_{k=1}^{K}\mathbb{E}\{|\mathbf{h}_k(i)|^2\}\right). \end{aligned}\tag{26}$$

Differentiating (26) with respect to γ_i and setting the derivative to zero gives

$$\widehat{\gamma}_i^{(j)} = \frac{1}{K}\sum_{k=1}^{K}\mathbb{E}_{\mathbf{H}|\mathbf{Y}_{\mathrm{tf},\mathcal{P}};\mathbf{\Gamma}^{(j-1)}}\{|\mathbf{h}_k(i)|^2\}. \tag{27}$$

Using the *a posteriori* probability distribution function (PDF) $f(\mathbf{H}|\mathbf{Y}_{\mathrm{tf},\mathcal{P}};\widehat{\mathbf{\Gamma}}^{(j-1)}) \sim \mathcal{CN}(\boldsymbol{\mathcal{M}}^{(j)},\mathbf{\Sigma}^{(j)})$ [11], the conditional expectation in (27) simplifies to the update expression in (24). Subsequently, the expression for $\widehat{\mathbf{\Gamma}}^{(j-1)}$ can be substituted from (27) to obtain the *a posteriori* mean $\boldsymbol{\mathcal{M}}^{(j)} \in \mathbb{C}^{M_\tau N_\nu \times K}$ and covariance matrix $\mathbf{\Sigma}^{(j)} \in \mathbb{C}^{M_\tau N_\nu \times M_\tau N_\nu}$, respectively. The hyperparameter update in (27) is simplified using the *a posteriori* PDF, and it is given by (24). The E-step and M-step are iteratively executed until the change between consecutive hyperparameter estimates satisfies $||\mathbf{\Gamma}^{(j)} - \mathbf{\Gamma}^{(j-1)}||_F^2 \le \epsilon$, or the predefined maximum iteration count $M_{\max}$ is reached. The parameters $M_{\max}$ and ϵ are selected to ensure reliable convergence. Upon convergence, the *a posteriori* mean $\boldsymbol{\mathcal{M}}^{(j)}$ yields the DD-BML-based estimate $\widehat{\mathbf{H}}$ of the VLC channel matrix $\mathbf{H}$. The main takeaways from the complexity evaluation are as follows. The BL, DD-BML, and LMMSE exhibit a computational scaling of $\mathcal{O}\left(M_\tau^3 N_\nu^3\right)$, primarily driven by the inversion of an $[M_\tau N_\nu \times M_\tau N_\nu]$. In contrast, the orthogonal matching pursuit (OMP) approach incurs a worst-case complexity of $\mathcal{O}\left(M^3 N_P^3\right)$, driven by the repeated computation of an intermediate least-squares solution at each iteration.

BCRLB: Applying the vec$(\cdot)$ operator to (20) yields the received pilot vector $\mathbf{y}_v = \mathrm{vec}(\mathbf{Y}_{\mathrm{tf},\mathcal{P}}) \in \mathbb{C}^{MN_PK\times 1}$, represented as $\mathbf{y}_v = \mathbf{\Phi}_v\mathbf{h}_v + \overline{\mathbf{z}}_v$, where $\mathbf{\Phi}_v = (\mathbf{I}_K \otimes \mathbf{\Phi}) \in \mathbb{C}^{MN_PK\times M_\tau N_\nu K}$, the stacked channel vector is $\mathbf{h}_v = \mathrm{vec}(\mathbf{H}) \in \mathbb{R}_+^{M_\tau N_\nu K\times 1}$, and $\overline{\mathbf{z}}_v = \mathrm{vec}(\mathbf{V}) \in \mathbb{C}^{MN_PK\times 1}$. Based on this model, the BCRLB quantifies the mean square error (MSE) of the estimated CIR. The Bayesian Fisher information matrix (FIM) for the channel prior and observation model is respectively, given by $\mathbf{J}_{h_v} = -\mathbb{E}_{\mathbf{h}_v}\left\{\frac{\partial^2\mathcal{L}(\mathbf{h}_v;\mathbf{\Gamma})}{\partial\mathbf{h}_v\partial\mathbf{h}_v^H}\right\}$ and $\mathbf{J}_{y_v} = -\mathbb{E}_{\mathbf{y}_v,\mathbf{h}_v}\left\{\frac{\partial^2\mathcal{L}(\mathbf{y}_v|\mathbf{h}_v)}{\partial\mathbf{h}_v\partial\mathbf{h}_v^H}\right\}$ [2], [11]. After simplification, the Bayesian FIM is obtained as $\mathbf{J} = \mathbf{J}_{h_v} + \mathbf{J}_{y_v} = (\mathbf{\Gamma}\otimes\mathbf{I}_K)^{-1} + \mathbf{\Phi}_v^H\mathbf{R}_v^{-1}\mathbf{\Phi}_v$. Thus, the BCRLB defining the achievable MSE bound of $\widehat{\mathbf{h}}_v$ is expressed as

$$\mathrm{MSE}(\widehat{\mathbf{h}}_v) \ge \mathrm{Tr}\left(\mathbf{J}^{-1}\right) = \mathrm{Tr}\left[(\mathbf{\Gamma}\otimes\mathbf{I}_K)^{-1} + \mathbf{\Phi}_v^H\mathbf{R}_v^{-1}\mathbf{\Phi}_v\right]^{-1}. \tag{28}$$

OMMSE: Under the assumption of perfect knowledge of the VLC channel delay profile, the OMMSE estimator is formulated as a benchmark reference. The oracle sensing matrix $\mathbf{O}_B = \mathbf{\Phi}(:,\mathcal{I})$ is formed by selecting the columns of $\mathbf{\Phi}$, where $\mathcal{I}$ denotes the support set of the non-zero channel coefficients obtained from the known sparse VLC channel delay profile. The resulting OMMSE estimate is given as [2]

$$\widehat{\mathbf{H}}_{\mathrm{OE}} = \left(\mathbf{O}_B^H\mathbf{R}_v^{-1}\mathbf{O}_B + \mathbf{I}_{L_p}\right)^{-1}\mathbf{O}_B^H\mathbf{R}_v^{-1}\mathbf{Y}_{\mathrm{tf},\mathcal{P}}. \tag{29}$$

V. Simulation Results

This section presents a comparative performance analysis of the proposed DD-BML-based method against existing CIR estimation techniques, namely BL, FOCal Underdetermined System Solver (FOCUSS), OMP, and LMMSE [2], for DD-domain CSI recovery in multipath DCO-OTFS VLC systems. The evaluation considers BER, NMSE, and pilot overhead as key performance indicators. The BER quantifies detection reliability at the receiver using the estimated CIR. In the simulation setup, $\mathbf{R}_h = \mathbf{I}_{M_\tau N_\nu}$, while the SNR (in dB) is defined as $\text{SNR (dB)} = 10\log_{10}\left(\frac{1}{\sigma^2}\right)$. The DD-BML algorithm employs convergence parameters $\epsilon = 10^{-6}$ and $M_{\max} = 50$, such that $\| \widehat{\boldsymbol{\gamma}}^{(j+1)} - \widehat{\boldsymbol{\gamma}}^{(j)} \|_2 > \epsilon$ and $j < M_{\max}$, whereas the OMP threshold is fixed at 0.1. The FOCUSS

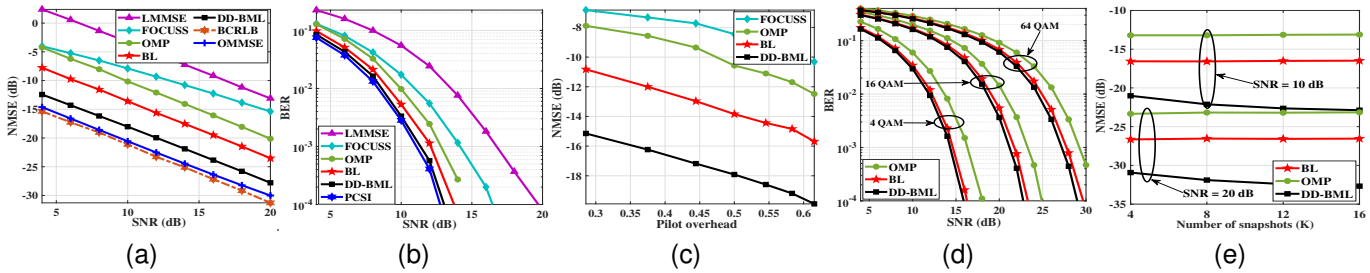

Fig. 1. DCO-OTFS VLC system, demonstrates (a) NMSE v/s SNR performance; (b) BER v/s SNR performance; (c) NMSE v/s pilot overhead (ρ) performance at SNR $= 10$ dB; (d) BER v/s SNR performance with higher-order modulation; (e) NMSE v/s number of snapshots (K).

configuration adopts a noise regularization factor σ^2, utilizes the l_p-norm with $p = 0.8$, and applies a termination criterion of 10^{-5} with a maximum of 800 iterations. The additional simulation parameters are set as $\Delta f = 240$ kHz, $M = 64$, $N = 64$, $N_p = 8$, $L = 16$, $L_p = 5$, $M_\tau = 32$, $N_\nu = 16$, $K = 5$, $B_{\text{DC}} = 7$ dB, modulation scheme is binary phase shift keying (BPSK), and pulse shape is rectangular [1], [2], [10].

Fig. 1(a) depicts the NMSE performance of the proposed DD-BML estimator in comparison with existing benchmark methods. The NMSE is evaluated as NMSE $= \frac{||\hat{\mathbf{H}}-\mathbf{H}||_F^2}{||\mathbf{H}||_F^2}$. By effectively exploiting the inherent sparsity of the channel, the DD-BML estimator achieves superior accuracy over LMMSE. Although OMP and FOCUSS are sparsity-driven techniques, their performance is constrained by sensitivity to tuning parameters and convergence behavior. The EM-based hyperparameter refinement in the DD-BML framework provides enhanced robustness against dictionary dependence and capitalizes on simultaneous sparsity across multiple snapshots. As a result, the proposed approach closely approaches the performance bounds defined by OMMSE and BCRLB. Fig. 1(b) presents the BER comparison, illustrating that the DD-BML scheme attains a significantly lower BER than the competing estimators and performs close to the ideal CSI benchmark, thereby validating its enhanced reconstruction efficiency. In the proposed framework, MN_P pilot symbols are transmitted in a block of $M(N + N_P)$ symbols, resulting in a pilot overhead of $\rho = \frac{N_P}{N+N_P}$. As illustrated in Fig. 1(c), DD-BML achieves uniformly lower NMSE across a broad range of ρ at SNR $= 10$ dB, while preserving strong bandwidth efficiency. In contrast, the embedded-pilot (EP) scheme requires $\rho_{\text{EP}} \approx \frac{(2M_\tau+1)(2N_\nu+1)}{MN}$ [12], which evaluates to $\rho_{\text{EP}} = 0.52$ versus $\rho = 0.11$ for the proposed method under the considered settings. This increased EP overhead arises from the DD-domain guard regions, which are eliminated by the proposed TF-grid pilot placement. Moreover, Fig. 1(d) depicts the BER performance for different quadrature amplitude modulation (QAM) orders (4, 16, and 64), where DD-BML consistently surpasses BL and OMP, minimizing training overhead without compromising estimation accuracy. In addition, Fig. 1(e) reports NMSE versus (v/s) the number of snapshots K (from 4 to 16), showing that DD-BML with 4 blocks achieves accuracy comparable to BL with 16 blocks. Hence, DD-BML enables efficient CE and improved BER with minimal pilot overhead in the DCO-OTFS VLC system.

VI. Conclusions

A simultaneous sparse CE scheme is proposed for DCO-OTFS VLC, where pilots are directly placed on the TF grid. This design reduces pilot overhead, training latency, and avoids a DD-domain guard interval between pilots and data, thereby improving bandwidth efficiency. The proposed DD-BML framework exploits DD sparsity together with simultaneous sparsity across multiple snapshots to enhance CE. The resulting CSI supports data detection without requiring knowledge of the number of dominant multipath components. Simulations demonstrate gains in NMSE, BER, and pilot efficiency over conventional CE schemes.

References

[1] C. Xu, X. Zhang, P. Petropoulos, S. Sugiura, R. G. Maunder, L.-L. Yang, Z. Wang, J. Yuan, H. Haas, and L. Hanzo, "Optical OTFS is capable of improving the bandwidth-, power-and energy-efficiency of optical OFDM," *IEEE Trans. on Commun.*, vol. 72, no. 2, pp. 938–953, 2023.

[2] S. Saxena, S. Srivastava, S. Sharma, A. K. Jagannatham, and L. Hanzo, "Sparse channel estimation for visible light optical OFDM systems relying on Bayesian learning," *IEEE Open J. Commun. Soc.*, vol. 4, pp. 2062–2079, 2023.

[3] R. Hadani, S. Rakib, M. Tsatsanis, A. Monk, A. J. Goldsmith, A. F. Molisch, and R. Calderbank, "Orthogonal time frequency space modulation," in *2017 IEEE Wireless Commun. and Netw. Conf. (WCNC)*. IEEE, 2017, pp. 1–6.

[4] P. Raviteja, E. Viterbo, and Y. Hong, "OTFS performance on static multipath channels," *IEEE Wirel. Commun. Lett.*, vol. 8, no. 3, pp. 745–748, 2019.

[5] J. Zhong, J. Zhou, W. Liu, and J. Qin, "Orthogonal time-frequency multiplexing with 2D Hermitian symmetry for optical-wireless communications," *IEEE Photonics J.*, vol. 12, no. 2, pp. 1–10, 2020.

[6] D. Zheng, H. Zhang, and J. Song, "DCO-OTFS-based full-duplex relay-assisted visible light communications," *Optics Express*, vol. 29, no. 25, pp. 41 323–41 332, 2021.

[7] A. Sharma, R. Mitra, O. Krejcar, K. Choi, M. Dobrovolny, and V. Bhatia, "Hyperparameter-free RFF-based post-distorter for OTFS VLC system," *IEEE Photonics J.*, vol. 15, no. 2, pp. 1–7, 2023.

[8] C. Cai, X. Hu, Z. Du, B. Zhu, W. Liao, X. Ma, B. Chen, Q. Chen, W. Ge, G. Song *et al.*, "A power-and spectrum-efficient underwater wireless optical communication system based on a hierarchical pre-distorted LACO-OTFS scheme," *J. Light. Technol.*, 2025.

[9] W. Chen, C. Ju, T. Yuan, J. Li, M. Zhang, and D. Wang, "Optical OTFS modulation for free space optical-based LEO satellite communication systems," *IEEE Photon. Technol. Lett.*, 2025.

[10] Y. Liao, J. Pei, W. Dai, J. Song, and Y. Dong, "Sparse Bayesian learning-based channel estimation for indoor OTFS visible light communication," in *2023 Asia Communications and Photonics Conference/2023 International Photonics and Optoelectronics Meetings (ACP/POEM)*. IEEE, 2023, pp. 1–5.

[11] D. P. Wipf and B. D. Rao, "An empirical Bayesian strategy for solving the simultaneous sparse approximation problem," *IEEE Trans. Signal Process.*, vol. 55, no. 7, pp. 3704–3716, 2007.

[12] P. Raviteja, K. T. Phan, and Y. Hong, "Embedded pilot-aided channel estimation for OTFS in delay-Doppler channels," *IEEE Trans. Veh. Technol.*, vol. 68, no. 5, pp. 4906–4917, 2019.